# NUMERICAL ANALYSIS OF ARTIFICIAL HYPERTHERMIA TREATMENT

## Łukasz Turchan, Ewa Majchrzak
Silesian University of Technology, Institute of Computational Mechanics and Engineering

*Abstract. This paper presents numerical modelling of artificial hyperthermia treatment. Presented model takes into account not only the temperature distributions but also the thermal dose parameter. Obtaining of temperature distributions takes advantage of the generalized dual phase lag equation. For computer calculations the parallelized algorithm was prepared.*

**Keywords**: artificial hyperthermia, finite difference method, parallelized calculations, dual phase lag model

## ANALIZA NUMERYCZNA ZABIEGU SZTUCZNEJ HIPERTERMII

*Streszczenie. Artykuł dotyczy numerycznego modelowania zabiegu sztucznej hipertermii. Analiza skuteczności zabiegu jest rozpatrywana nie tylko na podstawie czasoprzestrzennych rozkładów temperatury, ale także w oparciu o parametr dawki termicznej. Do modelowania przepływu ciepła w rozpatrywanym obszarze wykorzystano uogólnione równanie z dwoma czasami opóźnień. Na potrzeby obliczeń numerycznych napisano autorski program oparty o obliczenia równoległe.*

**Słowa kluczowe**: sztuczna hipertermia, metoda różnic skończonych, obliczenia równoległe, uogólnione równanie z dwoma czasami opóźnień

## Introduction

From the medical point of view hyperthermia is the sudden, rapid rise in a body temperature. Artificial hyperthermia is a treatment, in which the body temperature is purposeful raised, usually to 42 - 46 °C. There are three types of artificial hyperthermia: local, regional and whole-body. In this paper, only the local is considered. Local artificial hyperthermia is usually used as cancer treatment often associated with chemo - or radiotherapy. When this treatment is used unsupported, in cancer cells it causes lack of oxygen and nutrients, what leads to the apoptosis. Heat shock causes inducing of the heat shock proteins. Rise of temperature results in better blood supply to the organ and therefore drug accumulation. Chemical reactions are faster at higher temperatures. Artificial hyperthermia associated with the radiotherapy perpetuates damage of DNA.

It also should be noted, that the biological tissue is the material with particular nonhomogeneous inner structure and interwoven by blood vessels (Fig. 1). Sensitive influence on the temperature distribution has a volume of the blood vessels and blood velocity. The bioheat transfer process is multiscale, therefore it is necessary to consider delays of heat flux and temperature gradient [1].
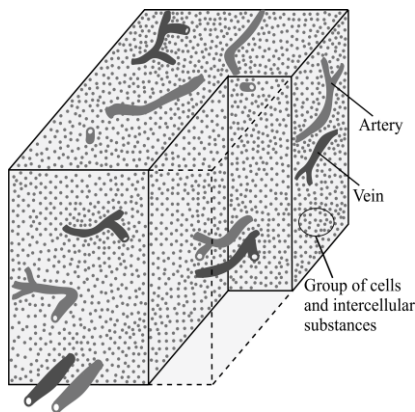


*Fig. 1. Tissue model*

To prevent damage of healthy tissue, as well heating the considered area to desirable temperature, the ability to predict the temperature distribution accurately, in a short calculation time is very important.

A model, which allows one to take into account the tissue porosity and phase lags depending on the parameters of tissue is the generalized dual phase lag model [11]. It should be pointed out that the comparison of various bioheat transfer models was done by authors in [8, 9].

It should be remembered that the degree of tissue destruction depends not only on the temperature, but also the exposure time and can be described mathematically by means of the thermal dose parameter [14].

## 1. Generalized dual phase lag equation

The tissue, as shown in figure 1, can be treated as a porous medium divided into two regions: the vascular region (blood vessel) and the extravascular region (tissue) [4, 11]. To describe temperature field in the heating regions (blood (1) and tissue (2)) the two-equation porous model [12] can be applied

$$(1-\varepsilon)\rho_t c_t \frac{\partial T_t}{\partial t} = (1-\varepsilon)\lambda_t \nabla^2 T_t + \alpha A (T_b - T_t) + \\ wc_b (T_b - T_t) + (1-\varepsilon)Q_{mt} + (1-\varepsilon)Q_{ex} \quad (1)$$

$$\varepsilon\rho_b c_b \left[ \frac{\partial T_b}{\partial t} + \mathbf{v} \cdot \nabla T_b \right] = \varepsilon\lambda_b \nabla^2 T_b + \alpha A (T_t - T_b) + \\ wc_b (T_t - T_b) + \varepsilon Q_{mb} + \varepsilon Q_{ex} \quad (2)$$

where ε denotes the porosity (the ratio of blood volume to the total volume), α is the heat transfer coefficient, **v** is the blood velocity, $A$ is the volumetric transfer area between tissue and blood, $c$ is the specific heat, ρ is the density, λ is the thermal conductivity, $T$ denotes temperature, $t$ is the time, $w$ is the blood perfusion rate, $Q_m$ is the metabolic heat source and $Q_{ex}$ is the capacity of internal heat sources associated with the external heating of tissue [9] while subscripts $t$ and $b$ represent tissue and blood, respectively. Adding both (1) and (2) equations, the following equation can be obtain

$$\varepsilon\rho_b c_b \frac{\partial T_b}{\partial t} + (1-\varepsilon)\rho_t c_t \frac{\partial T_t}{\partial t} + \varepsilon\rho_b c_b \mathbf{v} \cdot \nabla T_b = \varepsilon\lambda_b \nabla^2 T_b \\ + (1-\varepsilon)\lambda_t \nabla^2 T_t + \varepsilon Q_{mb} + (1-\varepsilon)Q_{mt} + Q_{ex} \quad (3)$$

In this paper is assumed that the coupling factor is equal to $G = A\alpha + wc_b$ and also that before reaching the equilibrium temperature of tissue and blood, the blood temperature changes according to the Minkowycz hypothesis [10]

$$\varepsilon\rho_b c_b \frac{\partial T_b}{\partial t} = G(T_t - T_b) \quad (4)$$

Based on (4) the temperature of tissue is described as follows

$$T_t = T_b + \frac{\varepsilon\rho_b c_b}{G} \frac{\partial T_b}{\partial t} \quad (5)$$

Using (5) and (3), after some mathematical operations the equation for blood temperature can be written in the form

$$\left[\varepsilon\rho_b c_b + (1-\varepsilon)\rho_t c_t\right]\frac{\partial T_b}{\partial t} + (1-\varepsilon)\rho_t c_t \frac{\varepsilon\rho_b c_b}{G}\frac{\partial^2 T_b}{\partial t^2} + \varepsilon\rho_b c_b \mathbf{v}\cdot\nabla T_b$$

$$= \left[\varepsilon\lambda_b + (1-\varepsilon)\lambda_t\right]\nabla^2 T_b + \frac{\varepsilon(1-\varepsilon)\lambda_t\rho_b c_b}{G}\frac{\partial}{\partial t}\left(\nabla^2 T_b\right) \quad (6)$$

$$+\varepsilon Q_{mb} + (1-\varepsilon)Q_{mt} + Q_{ex}$$

Now, the effectiveness parameters can be introduced:

$$\lambda_e = \varepsilon\lambda_b + (1-\varepsilon)\lambda_t \quad (7)$$

and

$$C_e = \varepsilon\rho_b c_b + (1-\varepsilon)\rho_t c_t \quad (8)$$

Assuming the following form of relaxation time and the thermalization time

$$\tau_q = \frac{\varepsilon(1-\varepsilon)\rho_t c_t\, \rho_b c_b}{G C_e} \quad (9)$$

$$\tau_T = \frac{\varepsilon(1-\varepsilon)\lambda_t\rho_b c_b}{G\lambda_e} \quad (10)$$

the equation (6) can be written as follows

$$C_e\left(\frac{\partial T_b}{\partial t} + \tau_q\frac{\partial^2 T_b}{\partial t^2}\right) + \varepsilon\rho_b c_b \mathbf{V}\cdot\nabla T_b = \lambda_e\nabla^2 T_b$$

$$+\lambda_e\tau_T\frac{\partial}{\partial t}\left(\nabla^2 T_b\right) + \varepsilon Q_{mb} + (1-\varepsilon)Q_{mt} + Q_{ex} \quad (11)$$

In equation (11) the unknown is the blood temperature. To determine the equation where only unknown is the tissue temperature the dependence (5) should be transform

$$T_b = T_t - \frac{\varepsilon\rho_b c_b}{G}\frac{\partial T_b}{\partial t} \quad (12)$$

Based on (11), (12) and after some mathematical operations the equation for tissue temperature is described as follows

$$C_e\left(\frac{\partial T_t}{\partial t} + \tau_q\frac{\partial^2 T_t}{\partial t^2}\right) = \lambda_e\nabla^2 T_t + \lambda_e\tau_T\frac{\partial}{\partial t}\left(\nabla^2 T_t\right) +$$

$$G(T_b - T_t) + \varepsilon Q_{mb} + (1-\varepsilon)Q_{mt} + Q_{ex} + \quad (13)$$

$$\frac{\tau_q C_e}{(1-\varepsilon)\rho_t c_t}\left[\varepsilon\frac{\partial Q_{mb}}{\partial t} + (1-\varepsilon)\frac{\partial Q_{mt}}{\partial t} + \frac{\partial Q_{ex}}{\partial t}\right]$$

## 2. Concept of thermal dose

Knowledge of time – dependent temperature field during the thermal treatment allows one to determine the thermal dose *TD* in terms of equivalent minutes at temperature 43°C. In particular, the following equation should be taken into account [14]

$$TD = \int_{t^0}^{t^F} R^{43-T}dt = \sum_{f=1}^{F} R^{43-T^f}\,\Delta t \quad (14)$$

where $t^0$, $t^F$ correspond to the initial and final times, respectively, $T^f$ is the temperature at the point considered for time $t^f$, $\Delta t$ is the time step, $R = 0$ for $T \le 39$ °C., $R = 0.25$ for 39 °C. $< T < 43$ °C. and $R = 0.5$ for $T \ge 43$ °C. The *TD* value required for total necrosis in a case of muscle tissue (this type of soft tissue is considered here) is equal to *TD* = 240 minutes [14].

## 3. Formulation of the problem

Assumed model is shown in figure 2. The domain of healthy tissue $\Omega_1$ is a cube with edge length of 0.05 m and centrally located subdomain of the tumor $\Omega_2$ with edge length of 0.01 m. The considered domain includes the blood vessels arranged in the direction of the X axis.

The thermophysical parameters of tumor and healthy tissue are assumed to be the same, so only one equation describing the temperature field in domain $\Omega = \Omega_1 \cup \Omega_2$ is considered. The external heating of tissue is a constant function

$$\begin{cases}(x,y,z)\in\Omega_1: \quad Q_{ex}(x,y,z,t)=0 \\[4pt] (x,y,z)\in\Omega_2: \quad Q_{ex}(x,y,z,t)=\begin{cases}Q_0, & t\le t_{ex}\\ 0, & t> t_{ex}\end{cases}\end{cases} \quad (15)$$

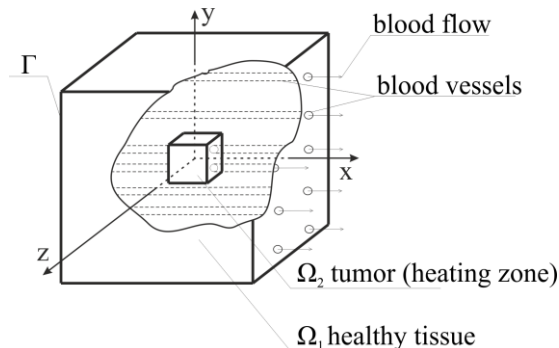where $Q_0$ is constant nonzero component and $t_{ex}$ is duration of heating (exposure time).



*Fig. 2. Domain considered*

## 4. Methods of solution

Assuming constant value of metabolic heat source and using formula (15) the equation (13) can be written in the form

$$C_e\frac{\partial T_t}{\partial t} + C_e\tau_q\frac{\partial^2 T_t}{\partial t^2} = \lambda_e\nabla^2 T_t + \lambda_e\tau_T\frac{\partial}{\partial t}\left(\nabla^2 T_t\right)$$

$$+G(T_b - T_t) + \varepsilon Q_{mb} + (1-\varepsilon)Q_{mt} + Q_{ex} \quad (16)$$

This equation is supplemented by boundary condition

$$-\lambda\, n\cdot\nabla T_t(x,y,z,t)=0 \quad (17)$$

where $n$ is the normal outward vector [3]. The initial conditions are as follows

$$t=0: \quad T_t(x,y,z,t)=T_p, \qquad \frac{\partial T_t(x,y,z,t)}{\partial t}=0 \quad (18)$$

where $T_p$ is the initial temperature of tissue. Let $T^f = T_t(x, y, z, f\Delta t)$ where $\Delta t$ is the time step [7]. Then, for time $t^f = f\Delta t$ $(f \ge 2)$ the following approximate form of equation (16) can be proposed

$$\frac{C(\Delta t + \tau_q)}{(\Delta t)^2}T^f = \frac{C(\Delta t + 2\tau_q)-G(\Delta t)^2}{(\Delta t)^2}T^{f-1}$$

$$-\frac{C\tau_q}{(\Delta t)^2}T^{f-2} + \frac{\lambda(\Delta t + \tau_T)}{\Delta t}\nabla^2 T^{f-1} - \frac{\lambda\tau_T}{\Delta t}\nabla^2 T^{f-2} \quad (19)$$

$$+GT_b + \varepsilon Q_{mb} + (1-\varepsilon)Q_{mt} + Q_{ex}$$

For simplification of notation the subscripts $t$ and $e$ are here omitted. The uniform grid of dimensions $n \times n \times n$ is introduced and then the finite difference equation for internal node $(i, j, k)$ has the following form [6]

$$\frac{C(\Delta t + \tau_q)}{(\Delta t)^2}T^f_{i,j,k} = \frac{C(\Delta t + 2\tau_q)-G(\Delta t)^2}{(\Delta t)^2}T^{f-1}_{i,j,k}$$

$$-\frac{C\tau_q}{(\Delta t)^2}T^{f-2}_{i,j,k} + \frac{\lambda(\Delta t + \tau_T)}{\Delta t}\nabla^2 T^{f-1}_{i,j,k} - \frac{\lambda\tau_T}{\Delta t}\nabla^2 T^{f-2}_{i,j,k} \quad (20)$$

$$+GT_b + \varepsilon Q_{mb} + (1-\varepsilon)Q_{mt} + Q_{ex}$$

where:

$$\nabla^2 T^s_{i,j,k} = \frac{T^s_{i-1,j,k} - 2T^s_{i,j,k} + T^s_{i+1,j,k}}{h^2}$$

$$+\frac{T^s_{i,j-1,k} - 2T^s_{i,j,k} + T^s_{i,j+1,k}}{h^2} + \frac{T^s_{i,j,k-1} - 2T^s_{i,j,k} + T^s_{i,j,k+1}}{h^2} \quad (21)$$

while $s = f - 1$ or $s = f - 2$ and $h$ is the constant grid step. Finally, the temperature at the node $(i, j, k)$ is calculated from

$$T_{i,j,k}^f = \frac{Ch^2\left(\Delta t + 2\tau_q\right) - Gh^2\left(\Delta t\right)^2 - 6\lambda\Delta t\left(\Delta t + \tau_T\right)}{Ch^2\left(\Delta t + \tau_q\right)}T_{i,j,k}^{f-1}$$

$$+\frac{\left(\Delta t\right)^2\left[GT_b + \varepsilon Q_{mb} + (1-\varepsilon)Q_{mt} + Q_{ex}\right]}{C\left(\Delta t + \tau_q\right)} \quad (22)$$

$$+\frac{\lambda\Delta t\left(\Delta t + \tau_T\right)\cdot dev1 - \lambda\Delta t\tau_T\cdot dev2 - \left(Ch^2\tau_q - 6\lambda\Delta t\tau_T\right)T_{i,j,k}^{f-2}}{Ch^2\left(\Delta t + \tau_q\right)}$$

where

$$dev1 = \left(T_{i-1,j,k}^{f-1} + T_{i+1,j,k}^{f-1} + T_{i,j-1,k}^{f-1} + T_{i,j+1,k}^{f-1} + T_{i,j,k-1}^{f-1} + T_{i,j,k+1}^{f-1}\right)$$
$$dev2 = \left(T_{i-1,j,k}^{f-2} + T_{i+1,j,k}^{f-2} + T_{i,j-1,k}^{f-2} + T_{i,j+1,k}^{f-2} + T_{i,j,k-1}^{f-2} + T_{i,j,k+1}^{f-2}\right) \quad (23)$$

It should be pointed out that in the case of explicit scheme application a criterion of stability should be formulated. The solving system is stable if the coefficients in the difference equations (22) for time $t^{f-1}$ are non-negative. Hence it results that the following coefficient must be positive

$$\frac{Ch^2\left(\Delta t + 2\tau_q\right) - Gh^2\left(\Delta t\right)^2 - 6\lambda\Delta t\left(\Delta t + \tau_T\right)}{Ch^2\left(\Delta t + \tau_q\right)} \geq 0 \quad (22)$$

## 5. CPU parallel algorithm

All the time steps must be performed consecutively so the time loop can't be divided into the parallel calculation. Temperature calculations at all nodes in each time step are executed in three nested loops: in the $x$ direction, in the $y$ direction and in the $z$ direction. These calculations can be easily divided into the parallel because all temperatures at the points are calculated based on the $f - 1$ and $f - 2$ time steps. In figure 3 the example of parallelization of CPU calculations is shown. The number of threads "q" depends on the CPU cores.
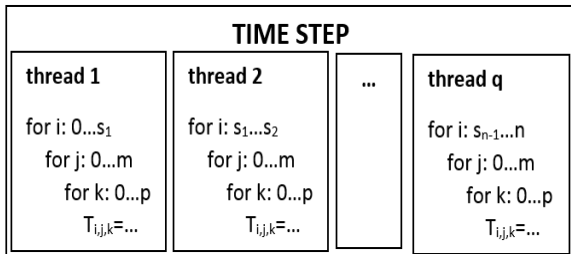


*Fig. 3. CPU parallelization of calculations*

## 6. GPU parallel algorithm

To achieve acceleration of computing time the CUDA technology of NVidia was implemented in computer program. This platform allows to use the graphics processing unit (GPU) for scientific computing. Unlike the CPU, the graphics processor is made up of hundreds of thousands cores (Fig. 4). Each of these cores may perform calculations independently.
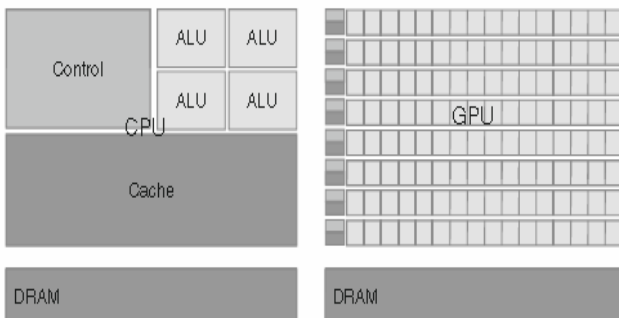


*Fig. 4. Model of CPU and GPU [5]*

The main limitation of graphics cards is the speed of copying data from the host to the device and the access time to data in the memory. The idea of using the GPU to accelerate the calculations associated with the finite difference method application is based on the fact that in each successive time steps the calculated data are new data for next time step, so it is not necessary to copy these data from the host to the device. The program algorithm is presented in figure 5.

The next very important factor which haves major impact on application efficiency is the idea of using shared memory. The global memory of the device has long access latencies and finite access bandwidth. Unlike to the previously, shared memory can be accessed at very high speed. The biggest problem in use of shared memory is limited amount of this memory [13].
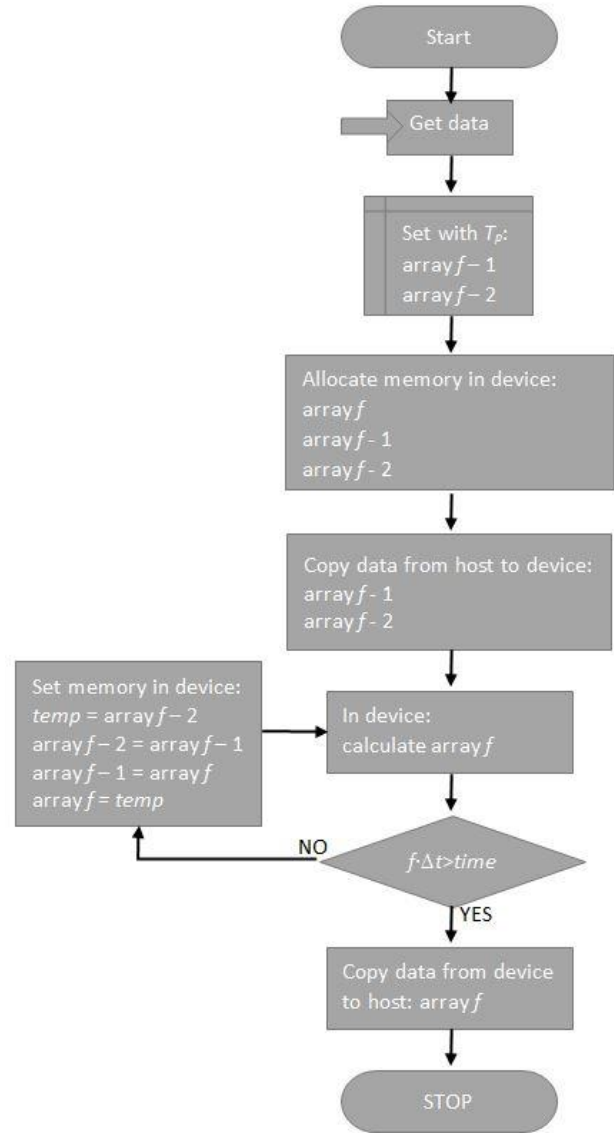


*Fig. 5. Algorithm*

Data for time steps $f$, $f - 1$ and $f - 2$ are stored in the memory as one dimensional arrays. In chosen approach each thread block loads a tile of data from those arrays. Proper choice of tile dimensions required some experimentations. It was decided to use a $4 \times 4 \times 25$ block size. Then for calculated all nodes temperature, the two arrays, in each threads blocks, from previous time steps of size $6 \times 6 \times 27$ are required (fig. 6).

The part of the code of the device kernel function, which copies the data from the global to the shared memory and calculates node temperature is shown on figure 7. After determining the temperature, for every node the thermal dose was also calculated.
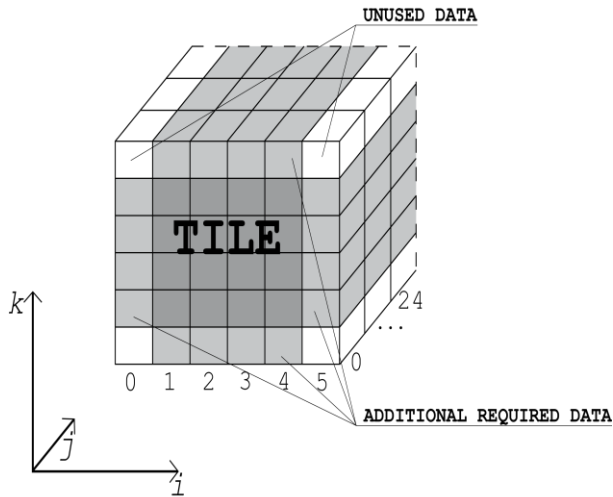
*Fig. 6. Array of data from f-1 time step in shared memory*

```
__global__ void TimeStepKernel(float
*arrF, const float
            *arrF1, const float *arrF2,
            Args arg)
{
__shared__ float sF1[6][6][27];
__shared__ float sF2[6][6][27];
int dimI = arg.dimI;
int dimJ = arg.dimJ;
int dimK = arg.dimK;
int tx = threadIdx.x;
int ty = threadIdx.y;
int tz = threadIdx.z;
int i = blockDim.x * blockIdx.x + tx;
int j = blockDim.y * blockIdx.y + ty;
int k = tz + arg.shift;

...
...

sF1[tx+1][ty+1][tz+1] =
arrF1[i*dimJ*dimK+j*dimK+k];
sF2[tx+1][ty+1][tz+1] =
arrF2[i*dimJ*dimK+j*dimK+k];
__syncthreads();

arrF[i*dimJ*dimK+j*dimK+k] =
   arg.A * sF1[tx+1][ty+1][tz+1] + arg.B
*
   (sF1[tx][ty+1][tz+1] +
sF1[tx+2][ty+1][tz+1] +
   sF1[tx+1][ty][tz+1] +
sF1[tx+1][ty+2][tz+1] +
   sF1[tx+1][ty+1][tz] +
sF1[tx+1][ty+1][tz+2]) -
   arg.C * (sF2[tx][ty+1][tz+1] +
sF2[tx+2][ty+1][tz+1] +
   sF2[tx+1][ty][tz+1] +
sF2[tx+1][ty+2][tz+1] +
   sF2[tx+1][ty+1][tz] +
sF2[tx+1][ty+1][tz+2]) - arg.D *
   sF2[tx+1][ty+1][tz+1] + arg.F + arg.E
* Qe;
__syncthreads();
```

*Fig. 7. Device kernel function*

## 7. Results

In numerical computations the following values of parameters have been assumed: thermal conductivity of blood $\lambda_b$, thermal conductivity of tissue $\lambda_t = 0.5$ W/(mK), blood density $\rho_b = 1060$ kg/m$^3$, tissue density $\rho_t = 1000$ kg/m$^3$, specific heat capacity of blood $c_b = 3770$ J/(kgK), specific heat capacity of tissue $c_t = 4000$ J/(kgK), metabolic heat source (of tissue and blood) $Q_{mb} = Q_{mt} = 250$ W/m$^3$, blood temperature $T_b = 37°C$, initial temperature $T_p = 37°C$, porosity $\varepsilon = 0.0137$ and $G = 27097.8$ W/(m$^3$ K). The values of phase lag times $\tau_q$ and $\tau_T$ were determined using formulas (9) and (10). The spatial discretization creates 500×500×500 nodes and time step is equal to $\Delta t = 0.01$ s. Following heating condition have been taken into account [9]: 35 s heating with a power density of 1 MW/m$^3$.

The program has been running on a computer with the processor Intel Core i7-3960X and the graphic card GeForce GTX 680. The processor has the six cores, each with two threads and the clock speed 3.3 GHz. The graphics processing unit has 1536 CUDA cores with base clock 1006 MHz and 2048 MB of global memory.

In figure 8 the temperature history at the central node of cube is presented. One can see that in the cube the maximum temperature 44°C. occurs and the temperature above 43°C is maintained only by 18 seconds.
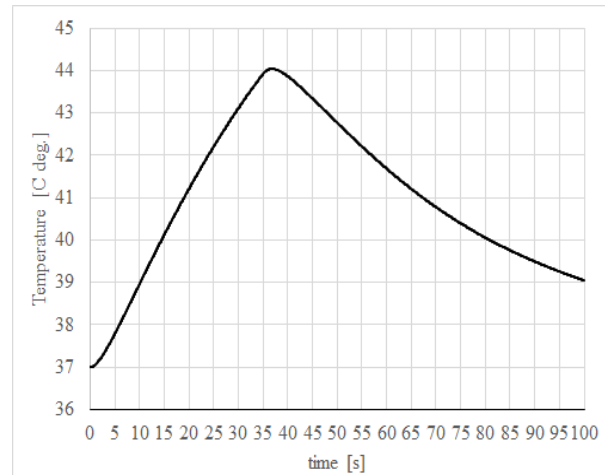


*Fig. 8. Temperature history at central node of cube*

Figure 9 illustrates the temperature distribution at the cross section ($z = 0$) after 10 second. The temperature above 37°C is just inside the tumor region.
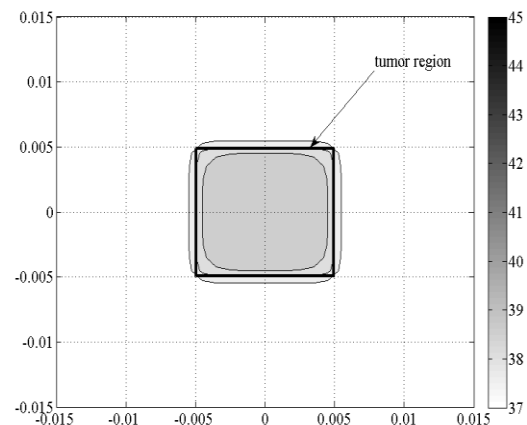


*Fig. 9. Temperature distribution at the central part of cross section after 10s*

In Figure 10 the temperature distribution in the cross section of the cube after 35 second is shown. In healthy tissue the temperature above 37°C appeared.
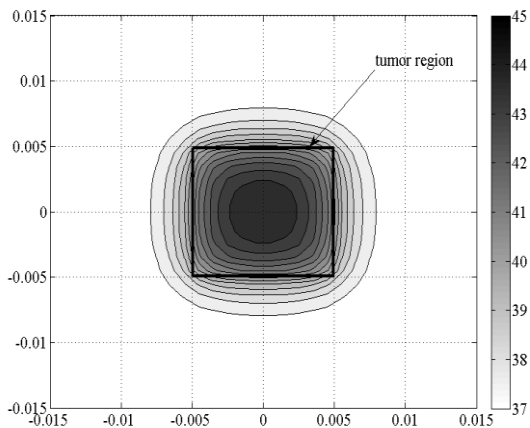


Fig. 10. Temperature distribution at the central part of cross section after 35s

After 60 seconds the temperature began to decrease – figure 11, but in the healthy tissue, there is still the temperature above 37°C. Also, more of the area $\Omega_1$ is occupied by the elevated temperature.
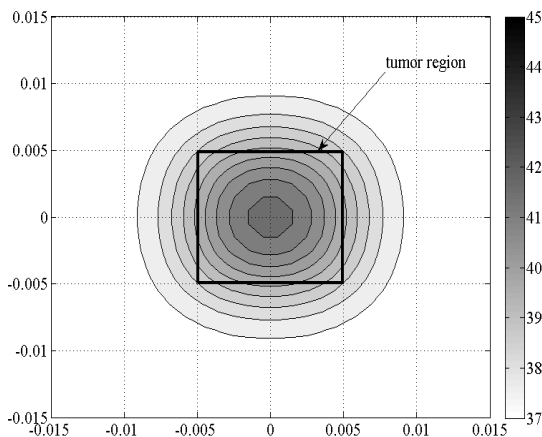


Fig. 11. Temperature distribution at the central part of cross section after 60s

After 100 seconds the temperature in the entire domain is less than 39°C (figure 12).
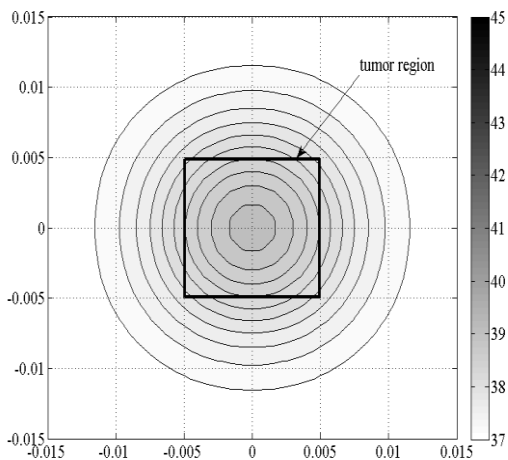


Fig. 12. Temperature distribution at the central part of cross section after 100s

In figure 13 the thermal dose history at the central node of the cube is presented. It is clearly that *TD* rise is meaningful in time from 25 to 60 seconds. After this time the thermal dose rise a little. It should be noted that values of thermal dose do not exceed 240 minutes.
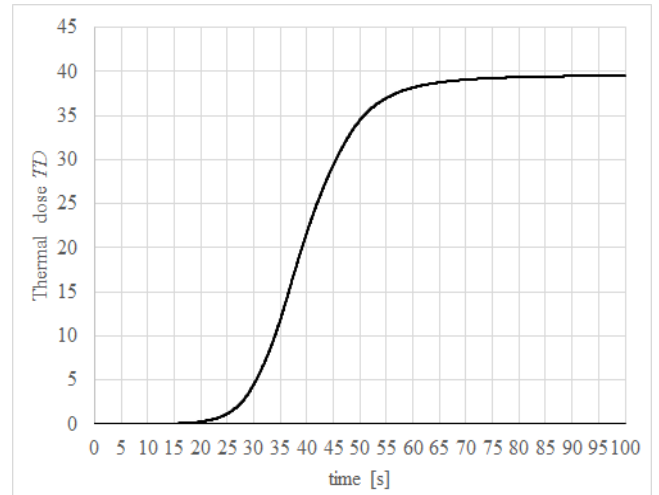


Fig. 13. Thermal dose history at central node of cube

In figure 14 the distribution of thermal dose in the central cross section is presented. It can be seen that all elevated values are inside the region $\Omega_2$.
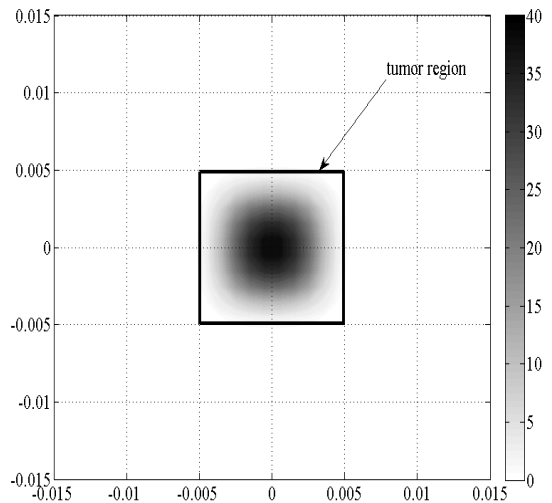


Fig. 14. Thermal dose distribution at the central part of cross section after 60s
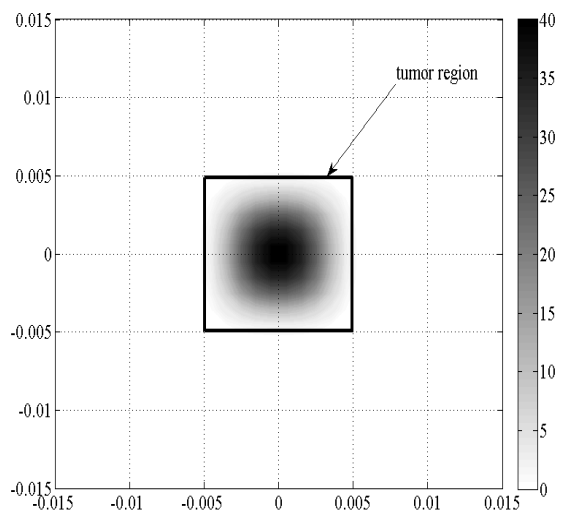


Fig. 15. Thermal dose distribution at the central part of cross section after 100s

Most important thermal dose distribution is after 100s because then the temperature decreases under 39°C and then the coefficient *R* in the thermal dose concept is equal to zero.

This distribution is presented in figure 15. It should be emphasized that all values of *TD* above 0 minutes are still inside the tumor region. This means that the healthy tissue is heated, but it does not receive a significant thermal dose.

As previously mentioned, the time step is equal to $\Delta t = 0.01$s, while the analysis time is equal to 100s. Thus, the amount of time steps is equal to 10,000. Assumed number of nodes is equal to $500 \times 500 \times 500$, so the number of temperatures which is necessary to calculate in each time step is equal to 125,000,000.

Computer program, which used only the CPU, all the calculations has been performed during 37 minutes and 43 seconds, at 95% of CPU utilization (Fig. 16).

Computer program which used not only CPU but also GPU, the same calculations has been performed during 14 minutes and 1 second. As can be seen, the acceleration of calculations is very significant.
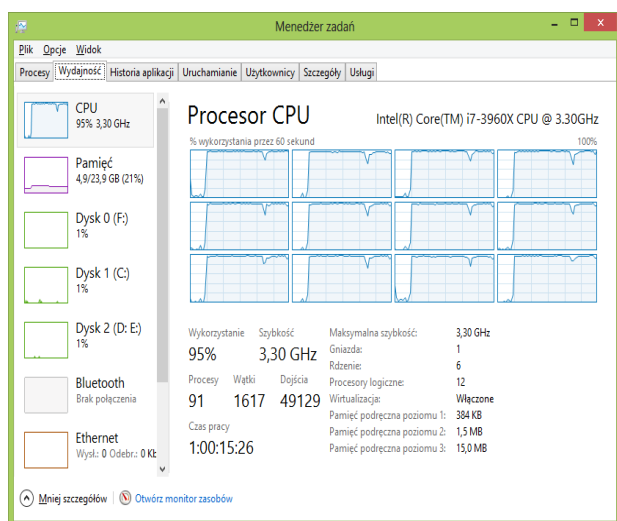


*Fig. 16. CPU utilization (without using CUDA)*

Table 1 provides a comparison of calculation times for different spatial discretizations. In all variants the same time step has been assumed. When changing the discretization for $100 \times 100 \times 100$ the tile sizes also have to be changed $(2 \times 2 \times 25)$, of course. The maximum difference between the results of the GPU and CPU calculations was below $1.6 \cdot 10^{-9}$.

*Table 1. Times of calculations*

| Spatial discret- ization | Calculation time | | Acceleration CPU / GPU |
|---|---|---|---|
| | GPU | CPU | |
| $500 \times 500 \times 500$ | 14min 1s | 37min 43s | 2,7 |
| $100 \times 100 \times 100$ | 8 s | 21 s | 2,5 |
| $50 \times 50 \times 50$ | 2,6 | 6,4 | 2,46 |

## 8. Results

In this paper the bioheat transfer process in three dimensional domain including the healthy tissue and the tumor region has been considered. Some simplifications were adopted, for example: very regular tumor shape and heating only in domain $\Omega_2$.

As can be seen in figures 9 – 12, the temperatures above 37°C. occur not only in the tumor, but also in the area of healthy tissue. During the treatment it is very important to prevent damage of healthy tissue and to provide adequate thermal dose in the tumor region. For a patient, the long duration of heating at high temperature will induce a feeling of discomfort and pain [8]. Based on the received thermal dose distribution it can be seen that not only the temperature is important, but also the exposure time. Figures 14 and 15 show that the thermal dose values above zero minutes are cumulated inside domain $\Omega_2$.

Using CUDA platform significantly speeds up the calculations. Calculations on graphics processing units should be implemented to the program, which repeatedly performs the complex analysis.

## Acknowledgements

## References

[1] Afrin N., Zhang Y., Chen J.K.: Thermal lagging in living biological tissue based on nonequilibrium heat transfer between tissue, arterial and venous bloods, International Journal of Heat and Mass Transfer, 2011, 54, pp. 2419–2426.

[2] Cattaneo C.: A form of heat conduction equation which eliminates the paradox of instantaneous propagation, Comp. Rend., 1958, 247, pp. 431-433.

[3] Ciesielski M.: Mochnacki B., Numerical analysis of interactions between skin surface temperature and burn wound shape, Scientific Research of Institute of Mathematics and Computer Science, 2012, 1(11), pp. 15-22.

[4] Khaled A.R.A., Vafai K.: The role of porous media in modeling flow and heat transfer in biological tissues, International Journal of Heat and Mass Transfer, 2003, 46, pp. 4989–5003.

[5] Kirk D.B., Wen-mei W. Hwu: Programming Massively Parallel Processors, Second Edition: A Hands-on Approach, Morgan Kaufmann, 2012.

[6] Majchrzak E.: Numerical modelling of bio-heat transfer using the boundary element method, Journal of Theoretical and Applied Mechanics, 1998, 2(36), pp. 437-455.

[7] Majchrzak E.: Mochnacki B.: Numerical methods. Theoretical bases, practical aspects and algorithms, Publ. of the Silesian University of Technology, Gliwice, Poland, 2004.

[8] Majchrzak E., Poteralska J.: Turchan Ł,: Comparison of different bioheat transfer models used in numerical modelling of a hyperthermia therapy, International Conference of the Polish Society of Biomechanics "Biomechanics 2010", Book of Abstracts, Warsaw, Poland, 2010, pp. 137-138.

[9] Majchrzak E., Turchan L.: Numerical modeling of a hyperthermia therapy using dual-phase-lag model of bioheat transfer, 19th International Conference on Computer Methods in Mechanics CMM 2011, Short Papers, Warsaw, Poland, 2011, pp. 337-338.

[10] Minkowycz, W.J., Haji-Sheikh, A., Vafai, K.: On departure from local thermal equilibrium in porous media due to a rapidly changing heat source: the Sparrow number, Int. J. Heat Mass Transfer, 42, 1999, pp. 3373-3385.

[11] Nakayama A., Kuwahara F.: A general bioheat transfer model based on the theory of porous media, International Journal of Heat and Mass Transfer, 51, 2008, pp. 3190–3199.

[12] Peng T., O'Neill D.P., Payne S.J.: A two-equation coupled system for determination of liver tissue temperature during thermal ablation, International Journal of Heat and Mass Transfer, 54, 2011, pp. 2100-2109.

[13] Wen-mei W. Hwu: GPU Computing Gems Emerald Edition, Morgan Kaufmann, 2011.

[14] Yuan, P.: Numerical analysis of temperature and thermal dose response of biological tissues to thermal non-equilibrium during hyperthermia therapy– Medical Engineering & Physics, 2008, 20, pp. 135-143.

**M.Sc. Eng. Łukasz Turchan**
e-mail: lukasz.turchan@polsl.pl

Łukasz Turchan is a PhD student at the Institute of Computational Mechanics and Engineering of Silesian University of Technology. His research interests focus on numerical methods and engineering computations. He is co-author of 15 publications and gave eight lectures at the national and international conferences. M.Sc. Turchan held an abroad internship in Vortex ICG Inc., Lawrence Technological University. He is a director of a research project funded by the National Science Centre.

**Prof. Ewa Majchrzak**
e-mail: ewa.majchrzak@polsl.pl

Ewa Majchrzak is a Deputy Director for Science at the Institute of Computational Mechanics and Engineering of Silesian University of Technology. She published over 400 papers, 5 books and 7 chapters in books. She is also supervisor of 11 Ph.D. theses. Her research interests include: computational science and engineering, heat and mass transfer, bioheat transfer, sensitivity analysis, inverse problems, boundary element method, multiscale heat transfer modelling and others. She is also member of many committee, scientific associations and four editorial boards.